Generalized Envelope-Based Modeling of Single-Phase Grid-Connected Power Converters

Francisco J. Azcondo, *Senior Member, IEEE*, Alberto Pigazo, *Senior Member, IEEE*, Christian Brañas, *Member, IEEE*, Paula Lamo, *Member, IEEE*, F. Javier Díaz, *Member, IEEE*, and Rosario Casanueva, *Member, IEEE*

***Abstract*—In-depth models of single-phase grid-tied power converters facilitate the examination of low-frequency (LF) interactions among loads, distributed energy resources (DERs), and synchronous generators by operators and designers. These interactions are becoming increasingly significant with the growing integration of power electronics into electrical grids. This article extends the envelope modeling (EM) technique to develop LF linear time-invariant (LTI) circuit models for single-phase grid-tied power converters. The models utilize an independent phase signal that aligns with the most appropriate reference frame. This methodology preserves the LF dynamics inherent to the power converter and control system. The practicality of this method is evidenced by constructing a model for a bridgeless totem-pole power factor corrector (PFC), which includes a zero-crossing detector (ZCD) and operates without closed-loop regulation. The outcomes from this model are juxtaposed with those from a switched model and other well-stablished modeling techniques for comparison. Furthermore, a commercially available circuit design featuring current and voltage control loops is simulated, and the results are corroborated with experimental data. These experiments are conducted under disturbances influencing the converter's performance within its linear operational range.**

***Index Terms*—Envelope modeling (EM), grid-connected converter, power factor correction (PFC).**

Manuscript received 31 August 2023; revised 18 December 2023 and 3 February 2024; accepted 7 March 2024. This work was supported in part by the EU Regional Development Fund (FEDER) and the Spanish Ministry of Science and Innovation under Research Project PID2021-128941OB-I00 (Efficient Energy Transformation in Industrial Environments) and in part by the Regional Government of Cantabria, Spain, and EU FEDER under Project 2023-TCN-008 UETAI. *(Corresponding author: Alberto Pigazo.)*

Francisco J. Azcondo, Christian Brañas, F. Javier Díaz, and Rosario Casanueva are with the Department of Electronics Technology, Systems and Automation Engineering (TEISA), Universidad de Cantabria, 39005 Santander, Spain (e-mail: azcondof@unican.es; branasc@unican.es; diaza@unican.es; casanuer@unican.es).

Alberto Pigazo is with the Department of Computer Science and Electronics, Universidad de Cantabria, 39004 Santander, Spain (e-mail: pigazoa@unican.es).

Paula Lamo is with the School of Engineering and Technology, Universidad Internacional de La Rioja, 26006 Logroño, Spain (e-mail: paula.lamo@unir.net).

Color versions of one or more figures in this article are available at https://doi.org/10.1109/TIE.2024.3379631.

Digital Object Identifier 10.1109/TIE.2024.3379631

I. Introduction

THE increasing penetration of power electronics within electrical grids intensifies low-frequency (LF) interactions among loads, distributed energy resources (DER), and synchronous generators. It exacerbates the risk of instability in power grids [1], [2]. Threat assessment necessitates the evaluation of the time domain transient responses for diverse scenarios. Moreover, at the power converter side, LF corrective actions due to outer/slow control loops, such as DC voltage regulation in AC/DC converters or synchronization and active-reactive droop control in DC/AC converters, induce interactions at the point of connection (PC) that warrant in-depth analysis [3], [4].

Most research efforts are focused on grid-connected power converters rated over tens of kilowatts. However, 1ϕ configurations, around 3.6 kW and below, dominate low-voltage (LV) residential grids. These configurations are used for home appliances, plug-and-play photovoltaics, domestic power storage, electric vehicles, and light mobility. Extracting LF characteristics in 1ϕ power converters is challenging since only one set of phase voltage and current measurements are available, and effects at twice the grid frequency have to be rejected for LF studies.

Analytical- and circuit-oriented approaches have been proposed for studying LF interactions in LV 1ϕ power systems under diverse scenarios. The target is to transform averaged models using the switching period of single-phase power converters into models retaining the most relevant characteristics of the controlled power converter to identify the interaction with the grid.

To address this problem, in [5], [6], and [7], the Park (dq) transformation is used to represent the grid voltage and line current in the rotating reference frame (RRF), which requires synchronization with the AC side of the power converter. An intermediate step is shifting the AC electrical quantities by 90°, i.e., one auxiliary imaginary orthogonal circuit (IOC) [8], [9], [10], [11], [12], or −120° and 120°, i.e., two auxiliary circuits [13], [14], to transform these quantities into the complex stationary reference frame (SRF). The resulting linear time-invariant (LTI) model in the RRF, under low harmonic distortion conditions or poor synchronization, is a *mildly periodic* system retaining most of the power converter characteristics [13]. The modeling approach can be extended to cope with

the harmonic distortion by using multiple dq transformations at integer frequency multiples of the fundamental. A phase-locked loop (PLL) is used or assists in transforming the electrical quantities into an RRF aligned with the grid voltage. So, the effects of the PLL dynamics cannot be studied independently.

Recently, dynamic phasors (DPs) have been used for modeling 1ϕ power converters for a certain set of frequencies of interest. In [15], DPs allow LF interactions of the electrical grid and 1ϕ PV inverters with active and reactive power control to be evaluated. Increasing the number of phasors permits the match of the dominant harmonics at both the AC and DC sides of the 1ϕ power converter, as in [16], [17]. DPs do not require grid synchronization since they correspond to time-varying coefficients for Fourier series expansions approximating *quasi-T*-periodic electrical quantities with a sliding time window length equal to $T=(2\pi/\omega_{DP})$, where each $k\in\mathbb{Z}$ multiple of ω_{DP} results in a k-order phasor [18], i.e.,

$$< X >_k = < x >_k^R + j < x >_k^I = \frac{1}{T}\int_{t-T}^{t} x(\tau)e^{-jk\omega_{DP}\tau}d\tau. \quad (1)$$

The resulting phasors avoid frequency overlapping and perform as stationary phasors in a steady state but retain slow amplitude and frequency variations of electrical quantities under dynamic conditions [19]. Windowing mismatches due to grid frequency variations might deteriorate the model performance, but under slow ones, the results are considered accurate enough [20], [21], [22].

Both the dq transformation and DPs, when used for modeling 1ϕ power converters, require a proper representation of the electrical quantities used for modeling purposes, which involves a certain previous knowledge about the grid angle or frequency and limits the performance of these methods for analyzing large frequency variations. The generalized envelope modeling (GEM) for 1ϕ grid-connected power converters presented in this article, whose basic equations were introduced in [23], avoids this issue through the key contribution of using a reference angle signal as an independent variable for AC quantities representation. Other contributions in Section II are the detailed derivation of the switching cell model and the evaluation of consistency with accepted power theories. Moreover, the GEM is compared with dq- and DP-modeling approaches in simulations, using a precalculated duty cycle to avoid biases due to the controller used, in Section III. This article also validates GEM experimentally with laboratory tests using a commercial evaluation board for a 1ϕ bridgeless totem-pole power factor corrector (PFC) in Section IV. Finally, conclusions are provided.

II. Generalized Envelope-Based Modeling (GEM) of Single-Phase Grid-Connected Power Converters

A. Electrical AC Quantities Representation

The GEM approach represents electrical AC quantities as time-varying phasors, e.g., $\bar{v}(t)$ and $\bar{i}(t)$. The notation in [24] and [25] is adopted here. The amplitude of each phasor retains

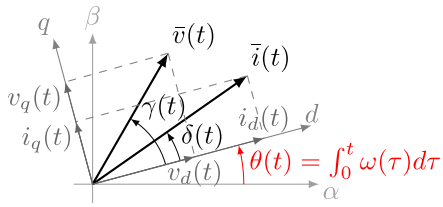

Fig. 1. Time-varying phasors of the grid voltage, the line current, and their representation in a certain set of SRF and RRF defined by the reference angle θ.

the whole spectrum of the represented electrical quantity, avoiding the decomposition and addition of the components at different frequencies. Phasors are initially considered uncorrelated and are represented using the same reference frame, and then, the relative position of $\bar{v}(t)$ and $\bar{i}(t)$ changes instantaneously depending on the frequency spectra, the actual grid frequency, and the converter operation. Having an infinite set of complex reference frames for the representation of $\bar{v}(t)$ and $\bar{i}(t)$, a certain SRF and RRF set, related through a certain angle θ, is selected, as depicted in Fig. 1. As a novelty, in this modeling approach, the positioning of these reference frames only depends on θ, i.e.,

$$\theta(t)=\int_0^t \omega(\tau)d\tau \quad (2)$$

which can be related or not to the electrical grid angle or frequency.

Despite the simplicity of (2), selecting the most appropriate θ is crucial to achieving a complete modeling of the interaction of the converters with the grid. While ω represents the switching frequency for resonant converters in [26] and θ would result from integrating ω, in this case, the model incorporates $\theta(t)$ from different origins depending on the study target, e.g., propagation of the power converter effects through the electrical grid.

From Fig. 1, the instantaneous AC quantities in that particular set of RRF and SRF are defined as

$$\begin{cases} v(t)=\mathcal{R}e\left\{\bar{v}(t)e^{j\gamma(t)}e^{j\theta(t)}\right\} \\ i(t)=\mathcal{R}e\left\{\bar{i}(t)e^{j\delta(t)}e^{j\theta(t)}\right\} \end{cases} \quad (3)$$

where $\bar{x}$ represents the amplitude and time-varying angles γ and δ depend on the relative position of the RRF and the voltage and current phasors, respectively. Then,

$$\begin{cases} \vec{v}(t)=\bar{v}(t)e^{j\gamma(t)}=v_d(t)+jv_q(t) \\ \vec{i}(t)=\bar{i}(t)e^{j\delta(t)}=i_d(t)+ji_q(t) \end{cases} \quad (4)$$

where d and q subscripts correspond to in-phase and in-quadrature quantities in the RRF, respectively. With (3), (4) is rewritten as

$$\begin{cases} v(t)=\frac{\vec{v}(t)e^{j\theta(t)}+\vec{v}^*(t)e^{-j\theta(t)}}{2} \\ i(t)=\frac{\vec{i}(t)e^{j\theta(t)}+\vec{i}^*(t)e^{-j\theta(t)}}{2}. \end{cases} \quad (5)$$

Given these AC quantities representations, large- and small-signal analysis can be carried out depending on the study target. Moreover, diverse values for $\omega(t)=\dot{\theta}(t)$ can be selected with this signal representation without deteriorating the dynamic information.

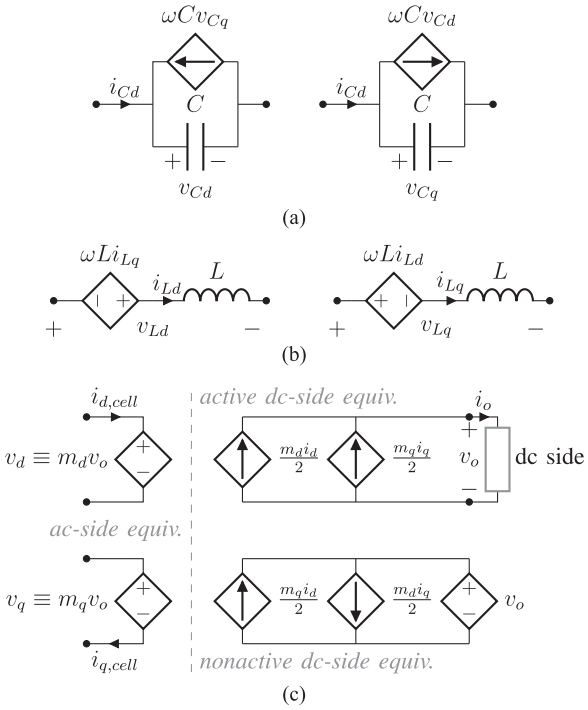

Fig. 2. Decoupled large-signal GEM of (a) AC capacitors in (8), (b) AC inductors in (9), and (c) AC/DC switching cells in (11) and (12).

B. AC Passives

Phasors in (4) enable the converter passives modeling without artificially influencing the obtained equivalent, as in dq- or DP-based methods, since the derivatives are obtained from the instantaneous AC quantities in (3). As in EM for resonant converters, if inductive and capacitive elements are used with the AC signal quantities in (5), the following relationships are obtained:

$$\frac{\vec{i}(t)e^{j\theta}+\vec{i}^{*}(t)e^{-j\theta(t)}}{2}=C\frac{d}{dt}\frac{\vec{v}(t)e^{j\theta}+\vec{v}^{*}(t)e^{-j\theta(t)}}{2} \tag{6}$$

$$\frac{\vec{v}(t)e^{j\theta}+\vec{v}^{*}(t)e^{-j\theta(t)}}{2}=L\frac{d}{dt}\frac{\vec{i}(t)e^{j\theta}+\vec{i}^{*}(t)e^{-j\theta(t)}}{2}. \tag{7}$$

From (6) and (7), two RRFs, at $\omega(t)$ and $-\omega(t)$, relate in-phase and in-quadrature components for capacitors and inductors at the AC side. Since the RRF at $-\omega(t)$ is a replica, the obtained relationships are given in the RRF at $\omega(t)$, i.e.,

$$\begin{aligned} i_{Cd}(t)+ji_{Cq}(t)&=C\frac{d}{dt}\left(v_{Cd}(t)+jv_{Cq}(t)\right)\\ &\quad+j\omega(t)C\left(v_{Cd}(t)+jv_{Cq}(t)\right), \end{aligned} \tag{8}$$

$$\begin{aligned} v_{Ld}(t)+jv_{Lq}(t)&=L\frac{d}{dt}\left(i_{Ld}(t)+ji_{Lq}(t)\right)\\ &\quad+j\omega(t)L\left(i_{Ld}(t)+ji_{Lq}(t)\right). \end{aligned} \tag{9}$$

Fig. 2(a) and 2(b) shows the equivalent inductor and capacitor models obtained from GEM for the RRF defined by the selected reference angle.

C. Switching Cells

The relationships between input and output electrical quantities depend on the switching cell topology and the gate signals. The instantaneous power at the AC side, $p(t)=v(t)i(t)$, is represented using the phasors in (5), resulting in

$$\begin{aligned} p(t)&=\underbrace{\frac{v_d(t)i_d(t)-v_q(t)i_q(t)}{2}}_{p_c(t)}\cos 2\theta(t)\\ &\quad-\underbrace{\frac{v_q(t)i_d(t)+v_d(t)i_q(t)}{2}}_{p_s(t)}\sin 2\theta(t)\\ &\quad+\frac{v_d(t)i_d(t)+v_q(t)i_q(t)}{2}=i_o(t)v_o(t). \end{aligned} \tag{10}$$

The last term in (10) inherently depends on the value $\theta(t)$ used to represent electrical quantities. It approximates the active power transferred $P(t)$, when $\dot{\theta}(t)=\omega(t)$ is close to the actual grid frequency. However, when $\dot{\theta}(t)$ deviates from the actual grid frequency, this term varies periodically depending on the frequency deviation and the frequency spectra of the phasors. The amplitude of the terms oscillating at $2\theta(t)$, i.e., p_c and p_s, depends on the AC phasors amplitudes and their relative angle, i.e., $|\gamma(t)-\delta(t)|$ in Fig. 1. For the proposed GEM, $\ddot{\theta}(t)\approx 0$, and then, $\dot{\theta}(t)=\omega$ varies slowly enough. Both the AC and the DC sides are linked through the power transferred, with $p(t)=i_o(t)v_o(t)$, where $i_o(t)$ and $v_o(t)$ are the DC current and voltage, respectively. The proposed GEM neglects the terms with amplitude $p_c(t)$ and $p_s(t)$ in (10) since those terms, depending explicitly on the reference frame set used, i.e., $2\theta(t)$, do not contribute to power transfer.

In the case of 1ϕ grid-connected power converters with capacitive DC bus, the AC voltage depends on v_o and the switching function used, i.e., $\vec{m}(t)=m_d(t)+jm_q(t)$, through

$$\vec{v}(t)=v_d(t)+jv_q(t)=\vec{m}(t)v_o(t) \tag{11}$$

where the frequencies of interest for the subsequent analysis are well below the switching frequency $f_{sw}=1/T_{sw}$. By replacing (11) into (10) and using GEM assumptions, the DC side current of the switching cell is obtained as

$$i_o(t)=\frac{m_d(t)i_d(t)+m_q(t)i_q(t)}{2}. \tag{12}$$

From (12), $i_o(t)$ depends on AC side quantities $\vec{m}$ and $\vec{i}$, exclusively.

For further clarification, the large-signal GEM is consistent with well-established electrical power theories [27], [28] and phasorial representations [29]. The Fryze–Buchholz–Depenbrock (FBD) theory [30] uses the averaged conductance, G, for the decomposition of the AC current into the component contributing to the active power i_p and the powerless current i_z as

$$i_p(t)=Gv(t)=\tfrac{P}{V^2}v(t)\quad\text{and}\quad i_z(t)=i(t)-i_p(t). \tag{13}$$

By replacing (5) into (13), the large-signal GEM equivalent of the FBD definitions is obtained as follows:

$$\vec{i}_p(t)=\tfrac{P(t)}{V^2(t)}\vec{v}(t)\quad\text{and}\quad\vec{i}_z(t)=\vec{i}(t)-\vec{i}_p(t) \tag{14}$$

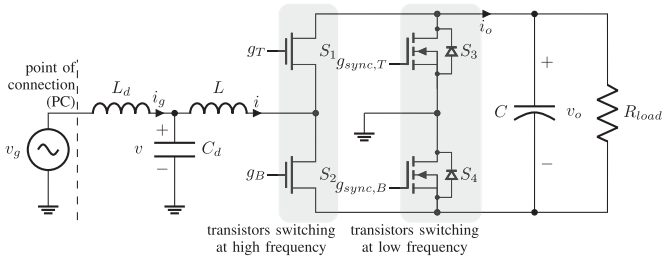

Fig. 3. 1ϕ bridgeless totem-pole PFC.

where $P(t) \approx (v_d(t)i_d(t) + v_q(t)i_q(t)/2)$, see (10) and the associated explanation, and the squared rms voltage V^2 is obtained from the squared voltage represented through the GEM, given (5), as

$$v^2(t) = \underbrace{\frac{v_d^2(t) - v_q^2(t)}{2}}_{v_c(t)} \cos 2\theta(t) - \underbrace{v_d(t)v_q(t)}_{v_s(t)} \sin 2\theta(t) + \frac{v_d^2(t) + v_q^2(t)}{2}. \tag{15}$$

Under the same assumptions as in (10), the first term in (15) inherently depends on the selected reference frame set while the two terms explicitly dependent on $2\theta(t)$ are neglected for $G(t)$ evaluation, i.e.,

$$G(t) = \frac{P(t)}{V^2(t)} = \frac{v_d(t)i_d(t) + v_q(t)i_q(t)}{v_d^2(t) + v_q^2(t)}. \tag{16}$$

Additionally, the large-signal GEM equivalent for the non-active power [28], N, is defined as

$$N(t) = \sqrt{S^2(t) - P^2(t)} = \frac{-v_d(t)i_q(t) + v_q(t)i_d(t)}{2} = \frac{-m_d(t)i_q(t) + m_q(t)i_d(t)}{2} v_o(t). \tag{17}$$

III. Comparison of Park, DP, and GEM Approaches

The dq and DP approaches, following the assumptions and procedures in [13] and [31], respectively, have been used for modeling the 1ϕ bridgeless totem-pole PFC depicted in Fig. 3. The switched model is simulated along with two dq, two DP, and two GEM models for validation and comparison purposes, using PLECS, from Plexim, and Simulink/MatLab, from Mathworks. The comparison uses the same conditions without a closed-loop controller.

A. Models Used for Comparison

Two dq-based models, DQ_{nom} and DQ_{PLL}, are tested using a SOGI PLL for AC quantities transformation to the RRF. However, DQ_{nom} uses the nominal grid frequency for AC variables decoupling, i.e., $\omega_{DQ} = \omega_0$ in Fig. 4(a) [13], while DQ_{PLL} uses the frequency estimation provided by the PLL, i.e., $\omega_{DQ} = \omega_{\text{PLL}}$.

Two DP-based models, DP_{simple} and DP_{full}, are also tested. DP_{simple} [Fig. 4(b)] uses first- and zeroth-order phasors with v_g, i_g, and v_o quantities, as in [31], in the averaged model of the 1ϕ bridgeless totem-pole PFC by assuming that $\omega_{DP} = \omega_0$ and, then, the fundamental or the DC component of these quantities. The model DP_{full} considers the DC side ripple at twice the grid frequency by including second-order phasor at the DC side, as shown in Fig. 4(c).

Two GEM, i.e., GEM_1 and GEM_2, with different complex reference frame sets are tested to validate the robustness of the proposal independently of the reference angle used, i.e.,

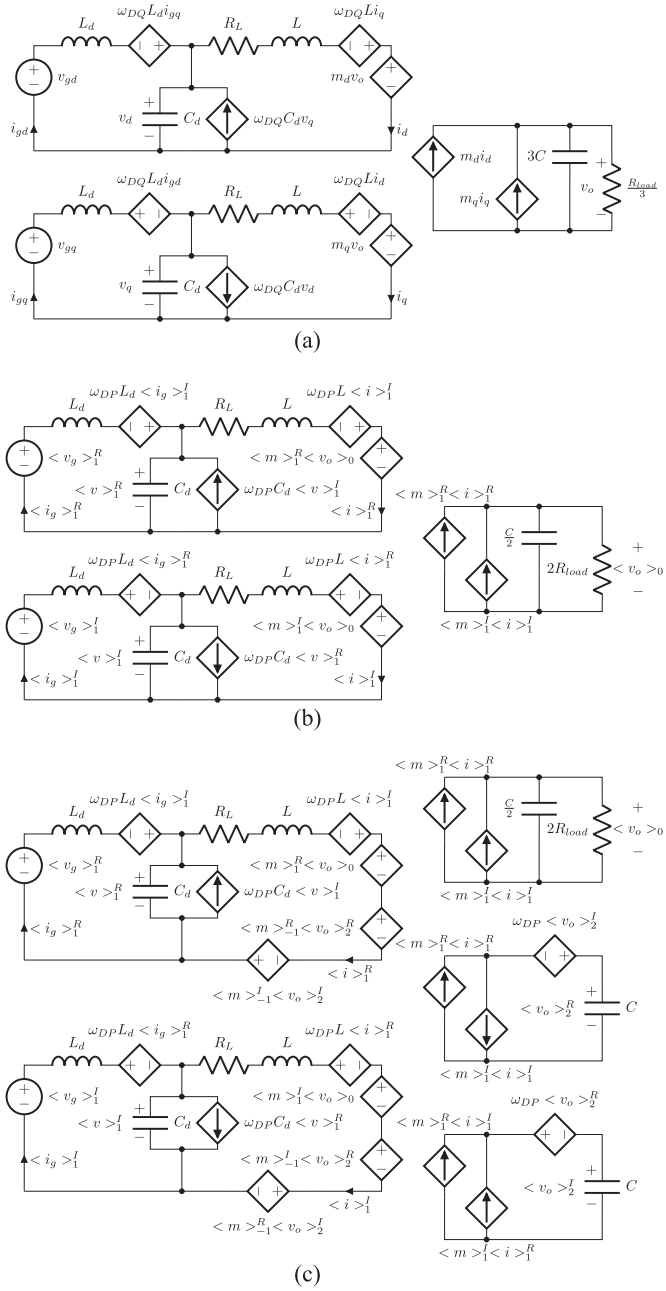

Fig. 4. Models of a 1ϕ bridgeless totem-pole PFC. (a) dq model, adapted from [13], (b) simple dynamic phasors-based model (with first- and zeroth-order phasors at AC and DC sides [31], respectively), and (c) full DP model of 1ϕ bridgeless totem-pole PFC (with first-order phasors at the AC side and zeroth- and second-order phasors at the DC sides).

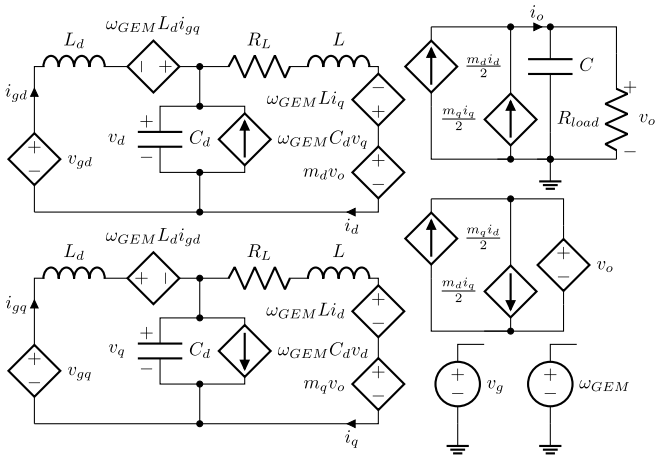

Fig. 5. Generalized envelope-based model of 1ϕ totem-pole PFC. Controlled voltage sources v_{gd} and v_{gq} depend on v_g and the selected ω_{GEM}.

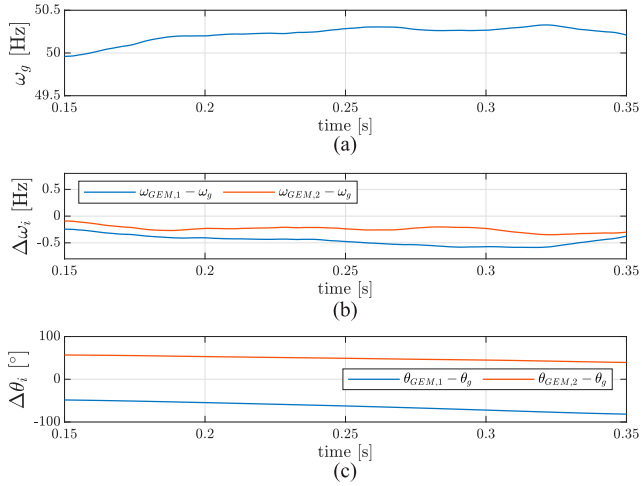

Fig. 6. Simulation conditions for open-loop tests. (a) Grid frequency. (b) Relative frequency. (c) Relative reference angle used for GEM.

the envelopes obtained are identical independently of the reference angle using the proposed GEM approach. Both GEMs follow the scheme depicted in Fig. 5, obtained by replacing the electrical quantities, passives and the switching cell at the AC side in Fig. 3 with GEM equivalents in Fig. 2. Passive components at the DC side are retained and connected to the active power port of the switching cell GEM equivalent. As a result, two AC-coupled circuits are obtained to represent the AC side while the DC side remains unchanged. The GEM presented demonstrates that perturbing the load results in model changes while perturbing the grid voltage, specifically v_{gq}, results in deterioration of the zero-crossing detection, producing model perturbations independently of the complex reference frame set selected. On the DC side, nonactive power interactions are also modeled.

B. Simulation Conditions

The grid frequency used, ω_g, for testing all the models is shown in Fig. 6(a). The reference angle for each GEM is obtained using (2), changing the initial conditions and using slightly different frequency profiles, as shown in Fig. 6(b) and 6(c) through $\Delta\omega_i = \omega_{\text{GEM},i} - \omega_g$ and $\Delta\theta_i = \theta_{\text{GEM},i} - \theta_g$, respectively. The frequency profiles are accomplished with EN-50 160 limits [32] and are obtained by adding a white noise sequence (0.005 pu power) filtered out through a 2.5 Hz second-order low-pass filter, which forces deviations of the complex reference frame set used for each GEM.

The models are compared using the precalculated duty cycle for power factor correction operation presented in [33].

LF switches, S_3 and S_4, are operated as diodes, and the high-frequency branch, S_1 and S_2, provides three-level PWM voltage at the AC side. High-frequency components in the line current are filtered out through an LCL filter, i.e., the boost inductor, L, and the differential LC due to the EMI filter, L_d and C_d. Precise zero-crossing grid voltage detection is required to achieve a low THD line current [34], [35]. Gate signals are routed to the power devices depending on the grid voltage polarity, i.e., $d = t_{\text{on}}/T_{sw}$ for S_2 during the positive grid semiperiod and S_1 during the negative semiperiod. Therefore, in this converter,

$$1 - d(t) = m(t)\text{sign}\left(\pi - \text{mod}\left(\frac{\theta_{\text{ZCD}}}{2\pi}\right)\right). \tag{18}$$

See that $(1-d)$ and m have the same envelope, so it is interesting to detect the effect of a phase perturbation linked to the rectification and polarity detection methods used.

Following standard design criteria for grid filters [36], [37], $v(j\omega) \approx v_g(j\omega)$ at approximately the grid frequency. Therefore, when the reference angle $\theta(t)$ is selected to match the electrical angle at the PC, the following relationship must be accomplished:

$$\vec{m} = \left(\left(\frac{1}{V_o} - \frac{V_o\left(R_{L_d} + R_L + R_{\text{meas}}\right)}{V_g^2 R_{\text{load}}}\right) - j\omega\frac{V_o\left(L_d + L\right)}{V_g^2 R_{\text{load}}}\right)\vec{v_g} \tag{19}$$

where the effects of C_d and grid-side harmonic distortion are neglected; unity power factor operation and small-ripple approximation for C (i.e., $v_o \approx V_o$) are assumed. Equation (19) includes the effects of parasitic inductor resistances, R_{Ld} and R_L, and the AC measurement resistor, R_{meas}. Parameters for comparison tests are given in Table I.

TABLE I
SIMULATION PARAMETERS FOR OPEN-LOOP COMPARISON OF dq, DP-MODELING AND GEM APPROACHES

L	R_L	C	R_{load}	V_o^{ref}	f_{sw}
5 mH	5 Ω	1.41 mF	340 Ω	390 V	100 kHz
$V_{g,\text{rms}}$	f_0	K_{SOGI}	$K_{P,\text{PLL}}$	$K_{I,\text{PLL}}$	EMI filter
230 V	50 Hz	$\sqrt{2}$	11.5	66.125	no

C. DC Load Step

A 340 Ω to 220 Ω load step is applied at 0.2 s. Fig. 7(a), 7(b), and 7(c) shows the simulation results for v_g, i_g, and v_o,

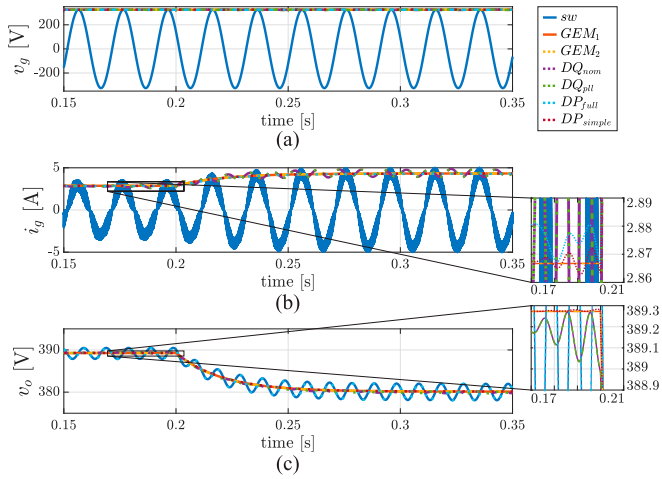

Fig. 7. Load step, from $R_L = 340\,\Omega$ to $220\,\Omega$, with open-loop controller. (a) AC voltage. (b) AC current. (c) DC voltage.

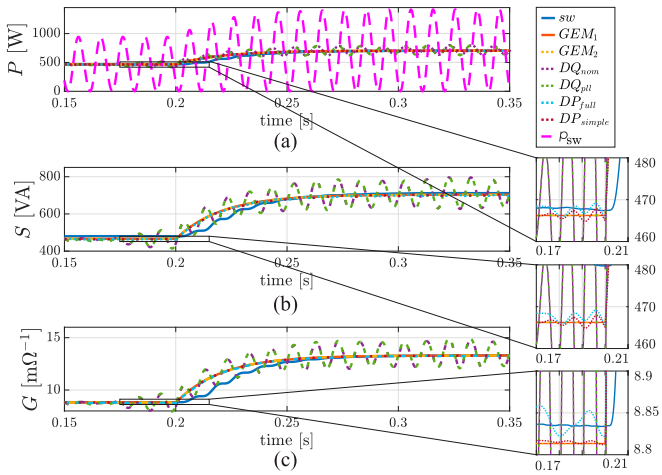

Fig. 8. Load step, from $R_L = 340\,\Omega$ to $220\,\Omega$, with open-loop controller. (a) Active power, P. (b) Apparent power, S. (c) Averaged conductance, G. Instantaneous power, p, for the switching model in dashed line.

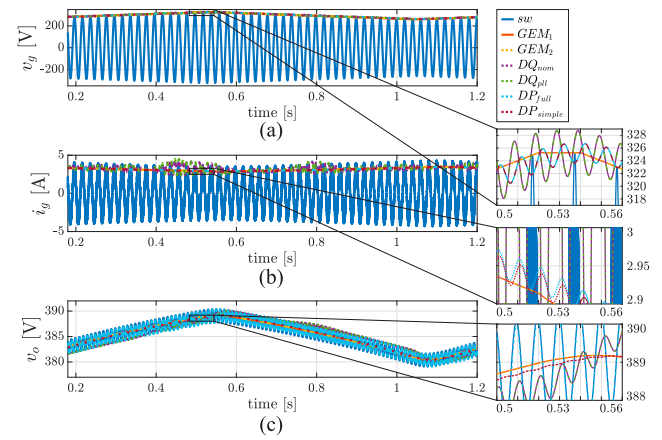

Fig. 9. Amplitude variations of the grid voltage, from 185 V to 230 V at 0.96 Hz, with a maximum 127.3 V s^{-1} slope, open-loop controller. (a) AC voltage. (b) AC current. (c) DC voltage.

TABLE II
COMPARISON OF LF MODELING APPROACHES FOR 1ϕ GRID-CONNECTED POWER CONVERTERS

	dq [13]	DP [31]	GEM
Initial approach	Circuital	Analytical	Circuital
Intermediate AC circuits	3	No	No
Intermediate DC circuits	3	No	No
Model complexity	Medium (aux. circ. + T_{dq})	$\propto$ num. of phasors (Fig. 4(b) & 4(c))	Low (5)
Complexity of passives tolerance analysis	Simple	$\propto$ num. of phasors	Simple
DC equiv. ratio	1/3	2	1
Effects of control loops at LF?	Yes	Yes	Yes
Frequency range	$[0, \frac{\omega_{RRF}}{2})$	$[0, N\omega_{DP})$	$[0, \omega_{GEM})$
AC synchronization	Required	Required	No (Figs. 6-9)
Decoupled synchronization analysis?	No	Yes	Yes
Upstream effects translation?	No	No	Yes (2)
Tolerance to w_g variations	Medium	Good	Best
Accuracy at LF (Figs. 7–9)	Good	Better	Best
Other analyses at $\omega > \omega_g$?	Yes, including more RRFs [38]	Yes, phasors for harmonics [17]	No
Frequency separation?	Yes, through ω_{RRF} for different RRFs	Yes, set of phasors	No, envelope of all freq. $< \omega_{GEM}/2$

Note: N: Max. phasor order in DP.

respectively. The GEMs result in envelopes following v_g and i_g amplitudes in the switching model. At the DC side [Fig. 7(c)], the GEM_1 and GEM_2 obtain the same output voltage, rejecting the oscillation at double the grid frequency and retaining the LF dynamics. DP_{simple} exhibits small amplitude oscillations due to the grid frequency variations. DP_{full} tracks the $2\omega_g$ ripple at the DC side, but the effect of the grid frequency variations is greater than DP_{simple}. Both DQ_{nom} and DQ_{pll} result in the highest ripple and error, DP_{pll} the worst, due to the large cutoff frequency of the PLL, i.e., $T_{settling} = 0.8$ s.

Fig. 8(a), 8(b), and 8(c) compares P, S, and G quantities with the same simulation conditions. The switching model evaluates them by averaging the instantaneous quantities with a sliding and adjustable window, minimizing errors due to the frequency profile used. A ripple-less and matching estimation of P, with differences below 0.3% in steady state, is obtained with both GEMs. The instantaneous power p due to the switching model is plotted in dashed line for the accuracy of GEM evaluating P. The computation of P from the switched model deviates from the actual value due to windowing mismatches while averaging the instantaneous quantities. Due to the grid frequency variations, DQ_{simple} and DQ_{pll} result in P with ripple. DP_{simple} and DP_{full} approximate the

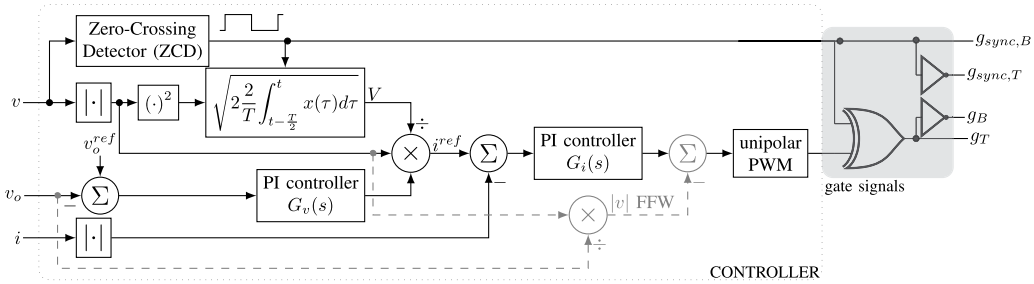

Fig. 10. Controller with rectified AC variables for 1ϕ bridgeless totem-pole PFC.

GEM performance but with ripple due to window length mismatches with the grid frequency. Differences among S evaluations due to the GEMs and the switched model increase to 1.4% [Fig. 8(b)], caused by high-frequency harmonics in the AC current, which the GEMs neglect. This effect worsens for DP_{simple} and DP_{full}, showing a ripple exacerbated by the grid frequency excursion from the nominal conditions. Again, DP_{simple} and DP_{full} approximate the GEM response but with ripple due to the window mismatch. From the average load conductance [Fig. 8(c)], the switched model and the values obtained with the GEM, i.e., (16), diverge less than 0.15% in steady state. The adjustable length of the averaging window used is the origin of larger response times of the evaluated electrical quantities due to the switching model. DP_{simple} and DP_{full} translate the ripple in P and S to the load conductance, while DP_{simple} provides a practical ripple-less conductance. On average, DP_{full} approximates the switched model conductance the best but exhibits the highest ripple of the DP and GEM models.

D. Low-Frequency Grid Voltage Amplitude Variations

The results for amplitude variations of the grid voltage, from 185 V to 230 V, at 0.96 Hz (a maximum 127.3 V s^{-1} slope) are shown in Fig. 9. The GEMs track both the AC and the DC variables retaining their LF characteristics up to ω_{GEM} without ripple, since envelope quantities are obtained for both semiperiods, i.e., twice the grid period. DP_{simple} and DP_{full} result in electrical quantities with ripple, depending on the grid frequency excursion. DP_{simple} approximates the most to the GEM responses, while DP_{full} exhibits a greater ripple. Moreover, from Fig. 9(c), the amplitude variations of v_g translate to the models, deviating the output voltage ripple from the switched model.

Table II compares key aspects due to dq, DP, and GEM approaches. Since the proposal is circuit-oriented, most analyses, such as component tolerance with Monte Carlo (MC), are enabled in a circuit-oriented simulation tool.

IV. Experimental Validation of the GEM

The 1ϕ bridgeless totem-pole PFC in Fig. 3 is controlled using the multiloop scheme in Fig. 10 for experimental validation of the GEM approach. The envelopes predicted by the GEM

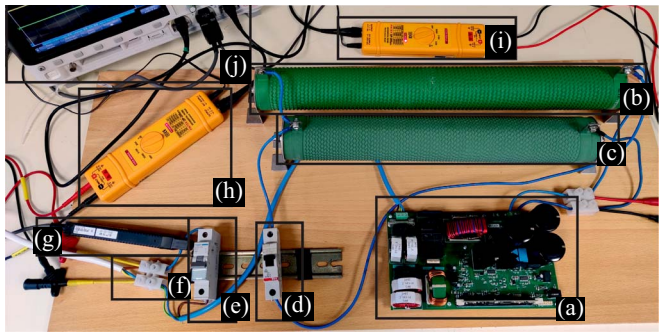

Fig. 11. Experimental setup. (a) 2.5 kW bridgeless totem-pole PFC transphorm TDTTP-2500P100. (b) 120 Ω 1.5 kW load. (c) 220 Ω 1.5 kW load. (d) Switch for DC load steps. (e) AC switch.(f) AC power source Pacific 345AMXT-UPC32. (g) Current probe Keysight N2783B. (h) and (i) Voltage differential probes Pintek DP-200pro. (j) 200 MHz oscilloscope Keysight DSOX3024T.

are compared with the electrical quantities obtained experimentally. The experimental setup is shown in Fig. 11. The current controller uses the rectified grid voltage and line current. Rectification is achieved with the help of a zero-crossing detector (ZCD), which identifies the grid voltage polarity and initializes the calculation of the rms value V as represented in Fig. 10 [39]. V is low-pass filtered with a first-order $f_{\text{cutoff}} \approx 4.5$ Hz filter. This value and the active power required by the power converter, evaluated through the outer voltage loop, i.e., $G_v(s)$, are used to obtain the average load conductance. The inner current controller, i.e., $G_i(s)$, is assisted by feedfowarding the AC voltage. The controller also implements antiwindup for the controller integrators, soft starting after zero voltage crossings for the active high-frequency switching power device. Power devices switching at the grid frequency are stopped when $|v_g|$ reaches a threshold voltage, i.e., $V_{g,\text{th}}$. Table III summarizes the most relevant operation parameters for the experimental tests.

The reference angle for GEM is obtained by integrating the grid frequency estimation given by the ZCD, i.e., $\theta(t) = \theta_{\text{ZCD}}(t) = \int_0^t (2\pi/T_{\text{ZCD}}(\tau))d\tau$, where T_{ZCD} is evaluated by counting the sampling periods between edges of the polarity signal.

A. DC Load Step

Fig. 12 shows the experimental results of the described setup with a 340 Ω to 220 Ω DC load step and the corresponding AC

TABLE III
PARAMETERS FOR EXPERIMENTAL VALIDATION OF GEM

L	500 µH	f_{sw}	100 kHz
$R_{\text{meas}} + R_L$	10 Ω	V_o^{ref}	390 V
C	1.41 mF	$K_{P,v}$	1335
R_{load}	340 Ω	$K_{I,v}$	7851
$V_{g,\text{rms}}$	230 V	$K_{P,i}$	0.0581
f_g	50 Hz	$K_{I,i}$	631.4
EMI filter	yes	$V_{g,th}$	4.32 V

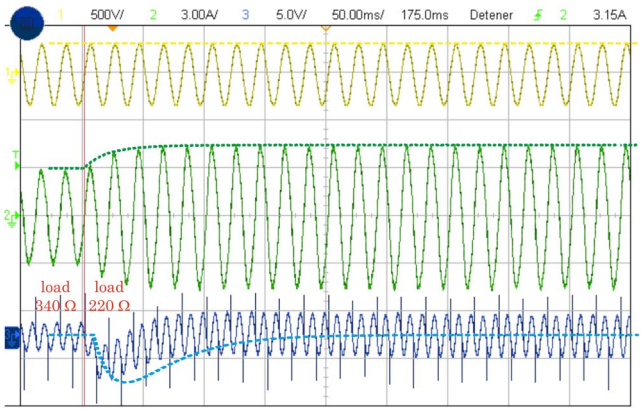

Fig. 12. Load step, from $R_L = 340\,\Omega$ to 220 Ω. Experimental: continuous, GEM: dashed. Input voltage (yellow, 500 V/div), input current (green, 3 A/div), and output voltage ripple (blue, 5 V/div). Time scale: 50 ms/div.

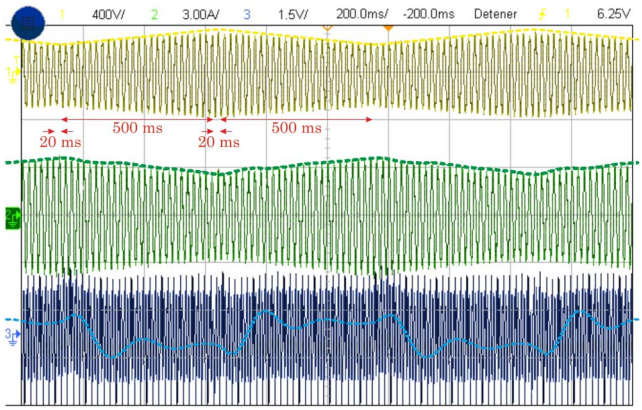

Fig. 13. Amplitude variations of the grid voltage, from 185 V to 230 V at 0.96 Hz, with a maximum 127.3 V s^{-1} slope. Experimental: continuous, GEM: dashed. Input voltage (yellow, 400 V/div), input current (green, 3 A/div), and output voltage ripple (blue, 1.5 V/div). Time scale: 0.2 s/div.

envelope and DC average variables obtained with the GEM. The GEM accurately follows the AC input voltage and current and predicts a 4.85 V output voltage drop with a 295 ms response time, close to the experimentally measured 260 ms. The deviation occurs because the step load transient contains high-frequency components that fall outside the modeling scope of the GEM. However, the controller employed by the evaluation board mitigates their impact, e.g., it prevents integrators wind-up.

B. Low-Frequency Grid Voltage Amplitude Variations

Fig. 13 shows the experimental results for amplitude variations of the grid voltage, from 185 V to 230 V at 0.96 Hz, with a maximum 127.3 V s^{-1} slope. On the AC side, the GEM retains LF variations of the grid voltage amplitude and LF effects on the line current. On the DC side, the effects of these variations, through the outer control loop, are also accurately captured.

V. CONCLUSION

An innovative approach to modeling single-phase grid-connected power converters, characterized by an envelope-based technique with an autonomous grid angle reference, has been introduced. This method facilitates the derivation of straightforward and precise LTI models for single-phase converters, applicable across both grid-following and grid-forming modes of operation. The technique is uniquely tailored for single-phase systems and aims to elucidate the dynamic interaction between the converter and the electrical grid. This concept was validated through comparative analysis of the envelope and switched models' steady-state and transient behaviors, focusing on voltage, current, and power metrics within a single-phase totem-pole PFC. This analysis was conducted independently of any synchronization mechanisms. Although the resulting circuit model resembles those derived via DPs or Park transformation, incorporating a grid angle reference and a distinct input parameter significantly mitigates transient and steady-state ripple discrepancies. Furthermore, empirical evidence from a prototype design corroborates the model's fidelity. The single-phase converter model notably encapsulates the LF phenomena attributable to the DC-side controller and the employed phase reference generation subsystem.

ACKNOWLEDGMENT

The authors would like to thank Plexim for facilitating PLECS®as simulation software.

REFERENCES

[1] X. Wang and F. Blaabjerg, "Harmonic stability in power electronic-based power systems: Concept, modeling, and analysis," *IEEE Trans. Smart Grid*, vol. 10, no. 3, pp. 2858–2870, May 2019.

[2] Y. Cheng et al., "Real-world subsynchronous oscillation events in power grids with high penetrations of inverter-based resources," *IEEE Trans. Power Syst.*, vol. 38, no. 1, pp. 316–330, Jan. 2023.

[3] X. Wang, M. G. Taul, H. Wu, Y. Liao, F. Blaabjerg, and L. Harnefors, "Grid-synchronization stability of converter-based resources—An overview," *IEEE Open J. Industry Appl.*, vol. 1, pp. 115–134, 2020.

[4] Y. Gu and T. C. Green, "Power system stability with a high penetration of inverter-based resources," *Proc. IEEE*, vol. 111, no. 7, pp. 832–853, Jul. 2023.

[5] J. Salaet, S. Alepuz, A. Gilabert, J. Bordonau, and J. Peracaula, "D-Q modeling and control of a single-phase three-level boost rectifier with power factor correction and neutral-point voltage balancing," in *Proc. 33rd Annu. IEEE Power Electron. Specialists Conf.*, Cairns, Australia, vol. 2. Piscataway, NJ, USA: IEEE Press, Nov. 2002, pp. 514–519.

[6] H. Sepahvand, M. Khazraei, K. Corzine, and M. Ferdowsi, "Start-up procedure and switching loss reduction for a single-phase flying capacitor active rectifier," *IEEE Trans. Ind. Electron.*, vol. 60, no. 9, pp. 3699–3710, Sep. 2013.

[7] M. Khazraei, H. Sepahvand, M. Ferdowsi, and K. A. Corzine, "Hysteresis-based control of a single-phase multilevel flying capacitor

active rectifier," *IEEE Trans. Power Electron.*, vol. 28, no. 1, pp. 154–164, Jan. 2013.

[8] R. Zhang, M. Cardinal, P. Szczesny, and M. Dame, "A grid simulator with control of single-phase power converters in D-Q rotating frame," in *Proc. 33rd Annu. IEEE Power Electron. Specialists Conf.*, Cairns, QLD, Australia, vol. 2. Piscataway, NJ, USA: IEEE Press, Jun. 2002, pp. 1431–1436.

[9] A. Roshan, R. Burgos, A. C. Baisden, F. Wang, and D. Boroyevich, "A D-Q frame controller for a full-bridge single phase inverter used in small distributed power generation systems," in *Proc. 22nd Annu. IEEE Appl. Power Electron. Conf. Expo.*, Anaheim, CA, USA, Feb. 2007, pp. 641–647.

[10] Y. Tang, Z. Qin, F. Blaabjerg, and P. C. Loh, "DQ reference frame modeling and control of single-phase active power decoupling circuits," in *Proc. IEEE Appl. Power Electron. Conf. Expo. (APEC)*, Piscataway, NJ, USA: IEEE Press, Mar. 2015, pp. 2725–2732.

[11] Y. Liao, Z. Liu, H. Zhang, and B. Wen, "Low-frequency stability analysis of single-phase system with dq-frame impedance approach—Part I: Impedance modeling and verification," *IEEE Trans. Ind. Appl.*, vol. 54, no. 5, pp. 4999–5011, Sep./Oct. 2018.

[12] S. Lee and S.-H. Lee, "DQ synchronous reference frame model of a series—Series tuned inductive power transfer system," *IEEE Trans. Ind. Electron.*, vol. 67, no. 12, pp. 10 325–10 334, Dec. 2020.

[13] Q. Lin, B. Wen, R. Burgos, X. Li, Q. Wang, and X. Li, "Input impedance modeling and experimental validation of a single-phase PFC in the D-Q frame," *IEEE J. Emerg. Sel. Top. Power Electron.*, vol. 10, no. 6, pp. 7371–7384, Dec. 2022.

[14] Q. Lin, B. Wen, R. Burgos, X. Li, Q. Wang, and X. Li, "D-Q impedance modeling and stability analysis of a three-phase four-wire system with single-phase loads," *IEEE Trans. Power Electron.*, vol. 38, no. 9, pp. 11169–11182, Sep. 2023.

[15] M. M. Koutenaei, T.-T. Nguyen, T. Vu, S. Paudyal, and R. Hovsapian, "Efficient phasor-based dynamic Volt/VAr and Volt/Watt analysis of large distribution grid with high penetration of smart inverters," *IEEE Trans. Smart Grid*, vol. 13, no. 5, pp. 3997–4008, Sep. 2022.

[16] U. C. Nwaneto and A. M. Knight, "Dynamic phasor-based modeling and simulation of a single-phase diode-bridge rectifier," *IEEE Trans. Power Electron.*, vol. 38, no. 4, pp. 4921–4936, Apr. 2023.

[17] U. C. Nwaneto and A. M. Knight, "Using dynamic phasors to model and analyze selective harmonic compensated single-phase grid-forming inverter connected to nonlinear and resistive loads," *IEEE Trans. Ind. Appl.*, vol. 59, no. 5, pp. 6136–6154, Sep./Oct. 2023.

[18] D. Maksimovic, A. Stankovic, V. Thottuvelil, and G. Verghese, "Modeling and simulation of power electronic converters," *Proc. IEEE*, vol. 89, no. 6, pp. 898–912, Jun. 2001.

[19] S. Sanders, J. Noworolski, X. Liu, and G. Verghese, "Generalized averaging method for power conversion circuits," *IEEE Trans. Power Electron.*, vol. 6, no. 2, pp. 251–259, Apr. 1991.

[20] Z. Shuai, Y. Peng, J. M. Guerrero, Y. Li, and Z. J. Shen, "Transient response analysis of inverter-based microgrids under unbalanced conditions using a dynamic phasor model," *IEEE Trans. Ind. Electron.*, vol. 66, no. 4, pp. 2868–2879, Apr. 2019.

[21] Y. Peng, Z. Shuai, X. Liu, Z. Li, J. M. Guerrero, and Z. J. Shen, "Modeling and stability analysis of inverter-based microgrid under harmonic conditions," *IEEE Trans. Smart Grid*, vol. 11, no. 2, pp. 1330–1342, Mar. 2020.

[22] Q. Peng, G. Buticchi, N. M. L. Tan, S. Guenter, J. Yang, and P. Wheeler, "Modeling techniques and stability analysis tools for grid-connected converters," *IEEE Open J. Power Electron.*, vol. 3, pp. 450–467, 2022.

[23] F. J. Azcondo, A. Pigazo, P. Lamo, and C. Branas, "Envelope-based modeling for single-phase grid-following and forming converters," in *Proc. IEEE 23rd Workshop Control Model. Power Electron. (COMPEL)*, Tel Aviv, Israel. Piscataway, NJ, USA: IEEE Press, Jun. 2022, pp. 1–6.

[24] C. Rim and G. Cho, "Phasor transformation and its application to the DC/AC analyses of frequency phase-controlled series resonant converters (SRC)," *IEEE Trans. Power Electron.*, vol. 5, no. 2, pp. 201–211, Apr. 1990.

[25] Y. Yin, R. Zane, R. Erickson, and J. Glaser, "Direct modeling of envelope dynamics in resonant inverters," in *Proc. IEEE 34th Annu. Conf. Power Electron. Specialist (PESC)*, Piscataway, NJ, USA: IEEE Press, 2003, pp. 1313–1318.

[26] Y. Yin, R. Zane, J. Glaser, and R. Erickson, "Small-signal analysis of frequency-controlled electronic ballasts," *IEEE Trans. Circuits Syst. I. Fundam. Theory Appl.*, vol. 50, no. 8, pp. 1103–1110, Aug. 2003.

[27] L. S. Czarnecki, "Effect of supply voltage harmonics on IRP-based switching compensator control," *IEEE Trans. Power Electron.*, vol. 24, no. 2, pp. 483–488, Feb. 2009.

[28] *IEEE Standard Definitions for the Measurement of Electric Power Quantities Under Sinusoidal, Nonsinusoidal, Balanced, or Unbalanced Conditions*, IEEE Std. 1459-2010.

[29] R.-Y. Kim, S.-Y. Choi, and I.-Y. Suh, "Instantaneous control of average power for grid tie inverter using single phase D-Q rotating frame with all pass filter," in *Proc. 30th Annu. Conf. IEEE Ind. Electron. Soc. (IECON)*, Busan, South Korea, vol. 1. Piscataway, NJ, USA: IEEE Press, 2004, pp. 274–279.

[30] V. Staudt, "Fryze - Buchholz - Depenbrock: A time-domain power theory," in *Proc. Int. School Nonsinusoidal Currents Compensation*, Lagow, Poland. Piscataway, NJ, USA: IEEE Press, Jun. 2008, pp. 1–12.

[31] U. C. Nwaneto and A. M. Knight, "Full-order and simplified dynamic phasor models of a single-phase two-stage grid-connected PV system," *IEEE Access*, vol. 11, pp. 26 712–26 728, 2023.

[32] *Voltage Characteristics of Electricity Supplied by Public Electricity Networks*, European Committee for Electrotechnical Standardization Std. EN 50 160, Dec. 2022.

[33] A. Sanchez, A. de Castro, V. M. Lopez, F. J. Azcondo, and J. Garrido, "Single ADC digital PFC controller using precalculated duty cycles," *IEEE Trans. Power Electron.*, vol. 29, no. 2, pp. 996–1005, Feb. 2014.

[34] M. Bhardwaj, S.-Y. Yu, Z. Ye, and S. Choudhury, "Improving light load power factor for GaN based totem pole bridgeless PFC using digital phase locked loop based vector cancellation and tracking error compensation," in *Proc. IEEE Appl. Power Electron. Conf. Expo. (APEC),* Piscataway, NJ, USA: IEEE Press, Mar. 2018, pp. 771–776.

[35] J. W.-T. Fan, R. S.-C. Yeung, and H. S.-H. Chung, "Optimized hybrid PWM scheme for mitigating zero-crossing distortion in totem-pole bridgeless PFC," *IEEE Trans. Power Electron.*, vol. 34, no. 1, pp. 928–942, Jan. 2019.

[36] M. Liserre, F. Blaabjerg, and S. Hansen, "Design and control of an LCL-filter-based three-phase active rectifier," *IEEE Trans. Ind. Appl.*, vol. 41, no. 5, pp. 1281–1291, Sep./Oct. 2005.

[37] K. Raggl, T. Nussbaumer, and J. W. Kolar, "Guideline for a simplified differential-mode EMI filter design," *IEEE Trans. Ind. Electron.*, vol. 57, no. 3, pp. 1031–1040, Mar. 2010.

[38] Y. Liao and X. Wang, "Small-signal modeling of AC power electronic systems: Critical review and unified modeling," *IEEE Open J. Power Electron.*, vol. 2, pp. 424–439, 2021. [Online]. Available: https://ieeexplore.ieee.org/document/9512447/

[39] "TDTTP2500P100-KIT: 2.5kW totem-pole PFC GaN evaluation platform." Transphorm. Accessed: Apr. 9, 2024. [Online]. Available: https://www.transphormusa.com/en/evaluation-kit/tdttp2500p100-kit/

Francisco J. Azcondo (Senior Member, IEEE) received the B.Eng. and M.Eng. degrees in electrical engineering from the Universidad Politécnica de Madrid, Madrid, Spain, in 1989, and the Ph.D. degree from the University of Cantabria, Santander, Spain, in 1993.

He was a Visiting Researcher with the Department of Electrical, Computer, and Energy Engineering, University of Colorado, Boulder, CO, USA, from 2004 to 2010; the Department of Electronics and Communication Engineering, University of Toronto, Toronto, ON, Canada, in 2006; and Utah State University Power Electronics Laboratory, Department of Electronics and Communication Engineering, Utah State University, Logan, UT, USA, in 2013. He is currently a Professor with the Department of Electronics Technology, Systems and Automation Engineering and the Dean of the Doctorate School, University of Cantabria. His current research interests include modeling and control of switch-mode power converters and resonant converters, digital control capabilities for switched-mode power supplies, and current sensorless control for grid-connected converters and applications, such as outdoor lighting, electrical discharge machining, and welding arc.

Dr. Azcondo was the Chair of the IEEE Industrial Electronics Society-Power Electronics Society Spanish Joint Chapter from 2008 to 2011. He has been an Associate Editor of IEEE JOURNAL OF EMERGING AND SELECTED TOPICS IN POWER ELECTRONICS and IEEE TRANSACTIONS ON INDUSTRIAL ELECTRONICS and the Vice Chair of IEEE PELS TC 1: Power & Control Core Technologies. He is an Associate Editor of IEEE TRANSACTIONS ON POWER ELECTRONICS.

Alberto Pigazo (Senior Member, IEEE) received the M.Sc. and Ph.D. degrees in physics (electronics) from the University of Cantabria, Santander, Spain, in 1997 and 2004, respectively.

He was a Guest Researcher with the Power Electronics Laboratory, Polytechnic of Bari, Bari, Italy, in 2007, and a Visiting Professor with the Department of Energy Technology, Aalborg University, Aalborg, Denmark, in 2013, and the Chair of Power Electronics, Christian-Albrecht University of Kiel, Kiel, Germany, in 2013. Since 2012, he has been an Associate Professor in electronics with the Department of Computer Science and Electronics, University of Cantabria. His current research interests include power converters for grid integration of renewable energy sources and power electronics for ships.

Christian Brañas (Member, IEEE) was born in Havana, Cuba, in 1970. He received the Ph.D. degree in electronics engineering from the Universidad de Cantabria, Santander, Spain, in 2001.

Currently, he is an Associate Professor in electronic technology with the Universidad de Cantabria. His current research interests include switch-mode power supply design, power factor correction circuits, and resonant power converters.

Paula Lamo (Member, IEEE) received the bachelor's degrees in naval engineering and marine engineering and the master's degrees in maritime engineering and teacher training from the University of Cantabria, Cantabria, Spain, in 2010 and 2011, respectively, the master's degrees in integrated management of environmental quality and occupational risk prevention and renewable energy from the University CEU San Pablo, Madrid, Spain, in 2012 and 2013, respectively, the master's and Ph.D. degrees in occupational risk prevention and industrial engineering from the University CEU San Pablo and the University of Cantabria, in 2014 and 2019, respectively.

Since 2014, she has been collaborating as a Researcher with the Department of Electronics Technology, Systems and Automation Engineering, University of Cantabria. She is currently an Associate Professor with the Universidad Internacional de La Rioja, Logroño, Spain.

F. Javier Díaz (Member, IEEE) was born in Torrelavega, Spain, in 1973. He received the B.S. degree in electrical and control engineering and the Ph.D. degree in industrial engineering from the University of Cantabria, Santander, Spain, in 1998 and 2009, respectively.

He has been a Professor with the Electronics Technology, Systems and Automation Engineering Department, University of Cantabria, since 1998. His research interests include designing, modeling, and control of switch-mode power converters for discharge lamps and topologies for power factor correction applications.

Rosario Casanueva (Member, IEEE) received the M.S. and Ph.D. degrees in physics from the University of Cantabria, Santander, Spain, in 1991 and 2004, respectively.

From 1991 to 1993, she worked on the design of highly stable quartz crystal oscillators. Since 1993, she has been an Assistant Professor with the Electronics Technology, Systems and Automation Engineering Department, University of Cantabria, where she has been an Associate Professor since 2011. Her research interests include switch-mode power supplies, grid-connected power converters, resonant converters and their control for electrical discharge generation, and battery energy storage applications.